Springer

Acta Mechanica Sinica

CrossMark click for updates

• RESEARCH PAPER •

Acta Mech. Sin., Vol. 40, 523282 (2024)
https://doi.org/10.1007/s10409-023-23282-x

A feasibility study on applying meta-heuristic optimization and Gaussian process regression for predicting the performance of pantograph-catenary system

Mohan Zhang[1,2], Bo Yin[1,2*], Zhenxu Sun[1,2], Ye Bai[3,4], and Guowei Yang[1,2]

[1] *Key Laboratory for Mechanics in Fluid Solid Coupling Systems, Institute of Mechanics, Chinese Academy of Sciences, Beijing 100190, China;*
[2] *School of Engineering Science, University of Chinese Academy of Sciences, Beijing 100049, China;*
[3] *Locomotive & Car Research Institute, China Academy of Railway Sciences Corporation Limited, Beijing 100081, China;*
[4] *Beijing Zongheng Electro-Mechanical Technology Co., Ltd., Beijing 100094, China*

Received September 14, 2023; accepted September 14, 2023; published online January 10, 2024

As the pantograph-catenary system provides electric energy for high-speed trains, it is vital to evaluate the contact force (CF) between pantograph and catenary for stable energy supply. The magnitude and variation range of CF determines the quality of current receiving and safe operation of the train. Therefore, a rapid and accurate prediction of CF is of great significance. However, collecting CF data through experiments is challenging, and obtaining timely results using numerical simulations is not always feasible. In this study, we propose an efficient simulation-based surrogate approach based on Gaussian process regression (GPR), combined with meta-heuristic optimization, to predict key parameters of pantograph-catenary system, which are responsible for the energy transfer quality. Firstly, a pantograph-catenary model is established and validated using finite element method (FEM), which serves to generate training and test data. Secondly, Gaussian process regression is utilized for estimation. A new developed meta-heuristic optimization, i.e., binary hunger game search (HGS), is applied on feature selection. To enhance the performance of HGS, chaos mechanism is embedded, resulting in Chaos-HGS GPR (CHGS-GPR). Finally, the predictive results of CHGS-GPR are evaluated. It is found that the proposed CHGS-GPR provides rather accurate prediction for the mean value of CF, and can be extended to the preliminary design of railway lines, real-time evaluation, and control of train operations.

Pantograph-catenary system, Gaussian process regression, Surrogate model, Physical-based model

Citation: M. Zhang, B. Yin, Z. Sun, Y. Bai, and G. Yang, A feasibility study on applying meta-heuristic optimization and Gaussian process regression for predicting the performance of pantograph-catenary system, Acta Mech. Sin. **40**, 523282 (2024), https:// doi.org/10.1007/s10409-023-23282-x

1. Introduction

Given the deteriorating state of the environment due to global warming, the transition to a low-carbon economy has become an inevitable trajectory for the development of all nations. Electricity, being a clean energy source, finds extensive application across various industries. China's electrified high-speed railway sector has experienced rapid growth in recent years, making a significant contribution to the global reduction of carbon emissions.

As the speed of high-speed trains increases, so does the demand for power units that provide the necessary traction. It is widely recognized that the pantograph serves as the interface for energy transfer from the overhead contact line. Consequently, the quality of contact between the pantograph and catenary assumes paramount importance in maintaining a stable power supply.

The contact force (CF) is a significant parameter used to evaluate the quality of the pantograph network [1]. On one hand, an excessively high CF accelerates wear and tear on the contact strip and pantograph network, leading to an undesirable reduction in its service life and increased mainte-

*Corresponding author. E-mail address: yinbo@imech.ac.cn (Bo Yin)
Executive Editor: Rui Huang

nance costs. On the other hand, an insufficient CF results in inadequate energy supply to the train and arcing between pantographs, which severely impacts the transmission quality. Hence, maintaining a consistently proper CF is crucial for pantograph-catenary system.

Measurement of the CF between the catenary and pantograph can be achieved through two primary methods: field measurements and numerical simulations. Field tests tend to be more expensive and challenging to carry out. Therefore, numerical simulation methods have gained wider adoption in recent decades. Finite element method (FEM) is primarily employed to model the catenary, while lumped mass and multi-body models are commonly utilized to represent pantograph. However, there is a limit to improving the computational efficiency of numerical methods based on physical models. They are unable to meet the requirements for rapid design and prediction of the pantograph-catenary system.

In recent years, there has been a growing interest in machine learning-based surrogate models, which are being increasingly explored to address complex real-world phenomena. In the field of railway engineering, researchers have started employing these techniques to develop surrogate models. Notable applications include the use of surrogate models to predict track degradation [2-6], as well as the deterioration of bearings [7, 8] and suspensions [9, 10] in vehicles. The utilization of digital twin technology in railway engineering often involves starting with existing experimental data, constructing surrogate models, and subsequently making predictions or performing diagnostics. In the context of the pantograph-catenary system, Huang et al. [11] were the first to evaluate the energy transfer quality of the system using a combination of a tree-based surrogate model and eight machine learning-based regression models. Their findings indicated that the multi-layer feed-forward deep residual neural network (MLF-DNN) model demonstrated the best performance.

Recently, stochastic surrogate models incorporating probabilistic analysis have exhibited impressive performance across various engineering domains. For instance, Hejazi et al. [12] utilized Gaussian process regression (GPR) to predict failure risks in steel catenary risers, yielding promising outcomes. In another study, Alruqi et al. [13] employed a GPR model to predict engine performance and exhaust emissions, achieving convincing results. Gautam et al. [14] conducted an experimental investigation on different geotechnical properties and modeled them using artificial neural network (ANN) and GPR models. Both machine learning methods demonstrated prediction errors within 10%, but the GPR-based model outperformed the ANN-based model in terms of percentage error. This is attributed to the fact that the ANN-based model tends to converge to locally optimal solutions, while the GPR-based model explores solutions across a wider range of response normal distributions. GPR facilitates rapid nonlinear regression prediction, enabling the estimation of the relationship between training data and predicted values in high-dimensional spaces [15]. Additionally, GPR provides confidence intervals, a capability lacking in other machine learning methods. The probabilistic nature of the GPR model renders it suitable for probabilistic and risk-based engineering assessments.

Building upon the advantages of the GPR model discussed earlier, we apply it to the pantograph-catenary system performance prediction, which, to the best of our knowledge, has not been attempted before. The objective of this paper is to evaluate the feasibility of adapting GPR to quantitatively predict the CF between pantograph and catenary. If the constructed approach is error-acceptable with affordable computational cost, then they are promising alternatives to traditional numerical simulation methods for pantograph and catenary energy transfer evaluation. The findings presented in this paper have implications for various railway engineering applications, including overall design, operation monitoring, and control of train operating. This work contributes in the following aspects: (1) A physics-based model is established and validated for training and testing data collection. (2) An attempt is made to use GPR combined with a modern developed meta-heuristic optimization on feature selection to predict the CF statistical results of pantograph-catenary system. (3) Parameters that have the most influence on the pantograph-catenary energy transfer performance can be concluded through the adopted feature selection method.

2. Methods

2.1 Pantograph-catenary system modeling

FEM is a widely used method to simulate the pantograph-catenary system, which has been well documented in many literature [16-24]. In this paper, the finite element software Abaqus [25] is used to build the model and simulate the system. Details are as follows:

Catenary is mainly composed of message wire (MW) , contact wire (CW) , suspensions, steady arms, and droppers. The sketch is shown in Fig. 1. MW and CW are modeled by beam units. In order to approximate the real situation, droppers are designed as a non-linear spring that can only be extended but not compressed. The structural damping of the contact network is modeled using a proportional damping model with values of $\alpha = 0.0125$ and $\beta = 0.0001$ [26]. To simplify the calculations, a commonly used three lumped mass model is adopted to represent the pantograph.

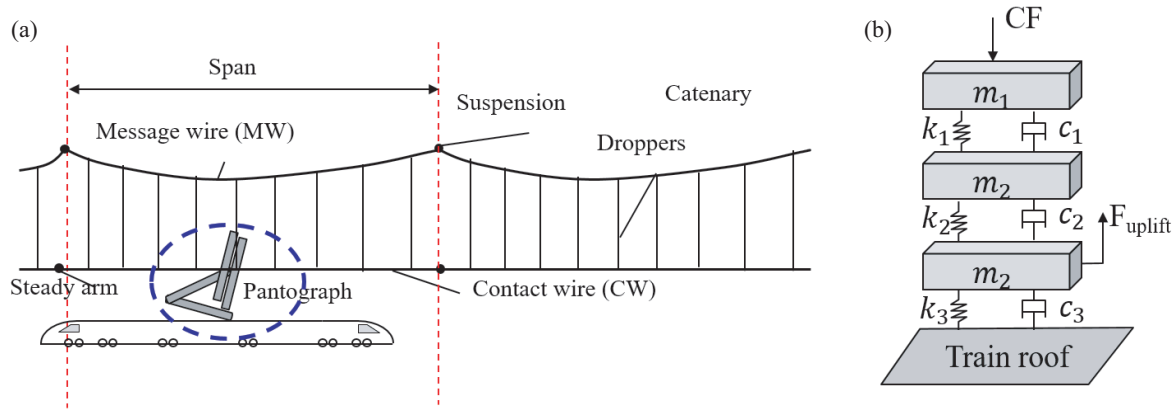

Figure 1 Description of (a) the catenary model and (b) the three lumped mass model of pantograph.

The model parameters are chosen in line with those in the workbench presented in Ref. [26]. The contact between pantograph and CW is modeled using a penalty function and is assumed to be frictionless. In this paper, a total of 10 spans of catenary are selected. In order to eliminate the influence of boundary effects, for the statistics of the results only the data of spans 5 and 6 are adopted.

The FEM model established in this paper is validated. Firstly, the accuracy of the model in predicting the initial sag length of CW has been verified. Figure 2(a) compares the results of present study with those of ten research institutes in the workbench [26] and the results are consistent with the reference. Secondly, the dynamic performance of the simulation has been verified. Figure 2(b) shows the dynamic contact forces and again the results agree very well with those in benchmark [26]. The statistical results are shown in Table 1. The difference of the minimum value is caused by the different modeling methods of steady arms, which falls into the acceptable range.

To further validate the accuracy of present FEM models, the reference model from European Standard EN 50318 [27] is used. The CF statistics are compared with the reference shown in Table 2. It can be seen that the current results are within the interval specified by the standard. Based on the above validation results, it can be concluded that the FEM models employed in this paper for simulating the pantograph-catenary system exhibit a reliable level of accuracy.

2.2 Gaussian process regression

GPR is a non-parametric supervised machine learning technique that uses prior information to estimate the posterior based on Bayesian inference. As an excellent kernel function-based strategy, GPR is suitable for handling datasets with many independent variables, small sample sizes, and a high degree of non-linearity. In GPR, the output y is related to the input x as follows:

$$y_i = f(x_i) + \epsilon_i, \tag{1}$$

where ϵ is the noise and f represents the unobservable potential function relationship. The noise is assumed to obey an independent identical Gaussian distribution with mean zero and variance is σ_n:

$$\varepsilon_i \sim \mathcal{N}(0, \sigma_n^2). \tag{2}$$

The key to GPR is the assumption that y obeys a joint Gaussian distribution:

$$y \sim \mathcal{N}(m(x), K(x, x)), \tag{3}$$

where $m(x)$ and $K(x, x)$ represent the mean and covariance matrix of $f(x)$, respectively. $K(x_i, x_i)$ is the covariance kernel function, representing the extent of correlation between two arbitrary sampled points. For simplicity, the mean value is usually set to 0. The goal of GPR is to infer the value of y^* at an unknown x^*, based on observations of x and y, which is, $p(y^*|y)$. By the assumptions of GPR, we know that y and y^* satisfy the joint Gaussian distribution, similarly:

$$\begin{bmatrix} y \\ y^* \end{bmatrix} \sim \mathcal{N}\left(\begin{bmatrix} 0 \\ 0 \end{bmatrix}, \begin{bmatrix} K & (K^*)^{\mathrm{T}} \\ K^* & K^{**} \end{bmatrix}\right), \tag{4}$$

where K is an n-dimensional matrix containing the covariance coefficients between observations, K^* is a vector containing the covariance coefficients between y_i and y^*, and K^{**} is y^*'s own covariance coefficient. Since $p(y^*\check{}y)$ is a Gaussian distribution, the mean and variance of the estimate y^* can be expressed as

$$(y^*)^\top = K^*(K^\top)^{-1}y, \tag{5}$$

$$\mathrm{var}(y^*) = K^{**} - K^*K^{-1}(K^*)^\top. \tag{6}$$

Cause the parameters affect the prediction accuracy. The Bayesian optimization method is applied to the selection of hyper-parameters.

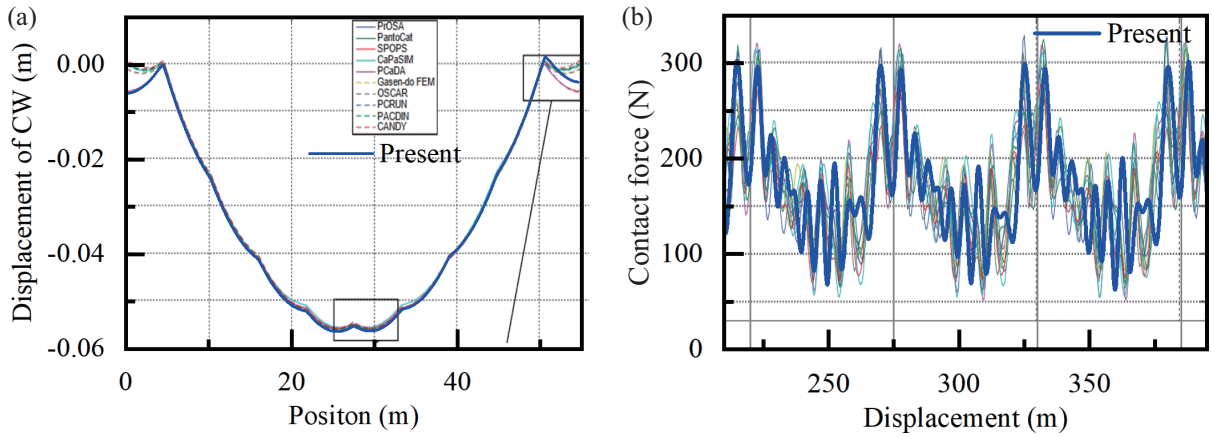

Figure 2 Verification of the present model against the results from benchmark: (a) the CW pre-sag and (b) CF.

Table 1 Present statistical results against the benchmark

	Benchmark	Present	Error
F_m (N)	169	168.6	0.2%
Std. (0-20 Hz) (N)	53.9	53.9	0%
Std. (0-2 Hz) (N)	38.3	38.9	1.6%
Std. (0-5 Hz) (N)	41.0	41.1	0.2%
Std. (5-20 Hz) (N)	34.8	35.0	0.5%
Max. (N)	313.2	299.4	4.4%
Min. (N)	60.4	67.7	12%

Table 2 Statistical results against EN 50318

	EN 50318		Present	
Speed (km/h)	250	300	250	300
F_m (N)	110-120	110-120	116.6	115.7
Std. (N)	26-31	32-40	28.3	34.2
Statistical max. (N)	190-210	210-230	201.5	218.5
Statistical min. (N)	20-40	–5-20	31.7	13.0
Actual max. (N)	175-210	190-225	182.2	190.0
Actual min. (N)	50-75	30-55	57.1	48.8
Max. uplift at support (mm)	48-55	55-65	53	55
Percentage of loss of contact (%)	0	0	0	0

3. Development of simulation based surrogates

Figure 3 illustrates the general framework of simulation based surrogates used in this paper. The purpose of building the simulation based surrogates in this paper is to make fast predictions of the quality of the pantograph-catenary energy transfer. Refer to the following sections for more details.

3.1 Problem description

The first thing that needs to be clarified for simulation based surrogates is to identify the variables to be predicted. Here, the objective of this paper is to predict the statistics of the dynamic contact forces between pantograph and catenary under a given system. The pantograph-catenary model used in this study and the outputs selected to evaluate the results are described below.

Firstly, the selection of the catenary model has been described in detail in Sect. 2.1. Then, the dynamic response of the pantograph-catenary interaction, including the pantograph CF and the CW uplift displacement at the joint between spans 5 and 6, is obtained by FEM numerical simulation. The two outputs have a significant impact on the quality of energy transfer and the safety of train operation [27]. According to the recommendations of the standard [28], the five basic parameters contain the mean CF (F_m), standard deviation (σ), maximum value ($F_{\max}$), minimum value ($F_{\min}$) and the uplift of the CW (U_{plift}) are the key indicators to judge the performance of the system. Therefore, these five output quantities are selected as the target parameters for determining the prediction accuracy of the prediction method.

3.2 Input parameters and sampling domain

The choice of input parameters and the calibration of their ranges have a great impact on the predictive and generalization capabilities of the surrogate models. In this study, independent variables (CW tension T_c, MW tension T_m, and train running speed v) are chosen to be input parameters. Also, the lifting force (F_{uplift}) applied to the pantograph is also taken into account. It is important to note that the range of values of F_{uplift} is related to the train speed [29], as shown in the following:

$$F_{m,\min} = 0.00047v^2 + 60, \tag{7}$$

$$F_{m,\max} = \begin{cases} 0.00047v^2 + 90, & \text{if } v \le 200 \text{ km/h}, \\ 0.00097v^2 + 70, & \text{if } v > 200 \text{ km/h}. \end{cases} \tag{8}$$

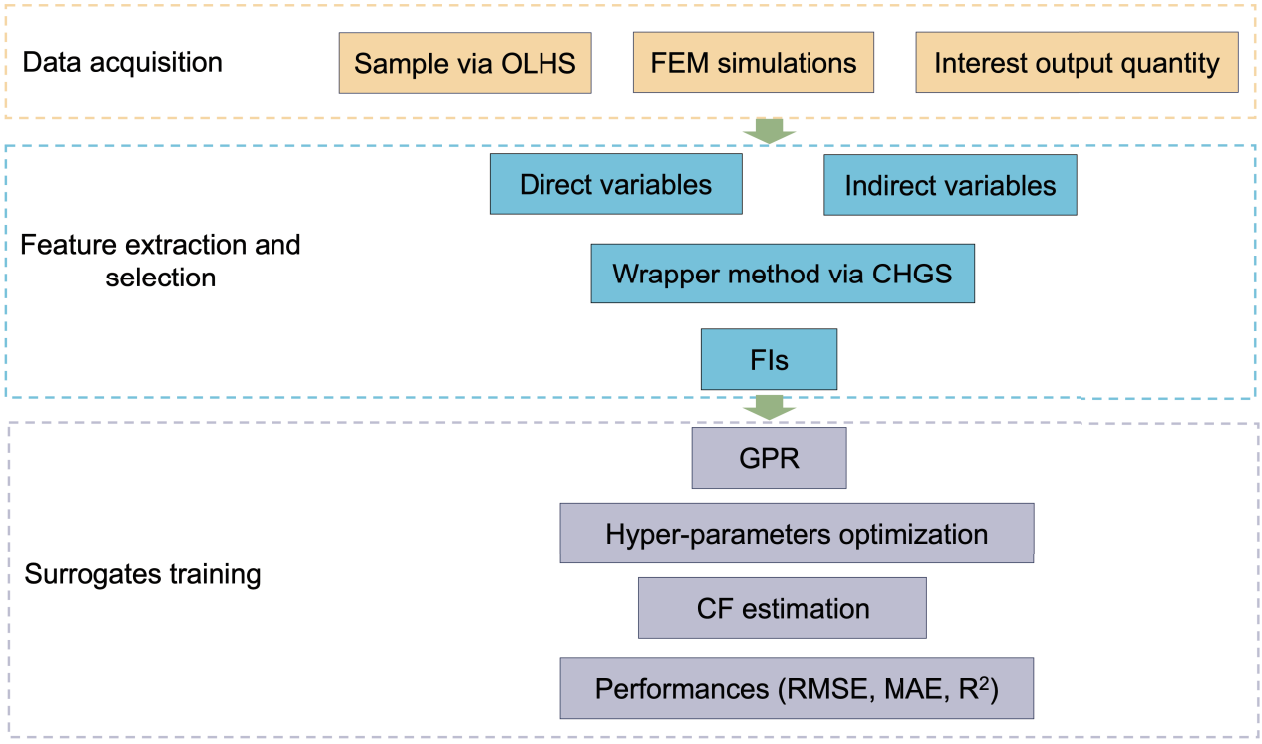

Figure 3 Framework of developing the simulation based surrogates.

According to some preliminary descriptions in the literature [30, 31], the key parameters responsible for the influence of CF may be the coefficients related to the reflection and transmission at the steady arms and dropper structures. With that under considered, this study derivates the CW reflection coefficient (C_{cr}), CW transmission coefficient (C_{ct}), MW transmission and reflection coefficient (C_{mr}) through the spectral analysis, and considers them as input parameters as well. The detailed derivation process is in Appendix A. In addition, the wave speed utilisation ratio of CW (defined as $\eta = v/c$, $c = \sqrt{T/\rho}$, c is the CW wave speed, T and ρ are CW tension and line density, respectively) is also added to input parameters. It should be noted that the three coefficients and η are related to the catenary inherent characteristics and the train operating conditions, therefore they are not independent variables here. In summary, the vector of input parameters used as an initial pre-selection for the training model is $\vec{X} = T_c, T_m, v, F_{\text{uplift}}, C_{cr}, C_{ct}, C_{mr}, \eta$.

Data plays a crucial role in the construction of surrogate models. The optimal Latin hypercube sampling (OLHS) strategy is used to reduce the effort and cost. Compared to traditional experimental design methods, the Latin hypercube design allows for a smaller number of test points to be used to fill the entire design space. However, the problem of uneven distribution of design points remains. Moreover, as the number of layers increases, it is easy to lose some areas in the design space. So the concept of OLHS was proposed. OLHS improves the homogeneity of the stochastic Latin hypercube design and makes the fitting of input and output variables more accurate and realistic [32]. OLHS allows for a uniform distribution of all test points with good space filling and balance. More information on OLHS can be checked in Ref. [33].

As can be seen from the above, in present study, T_c, T_m, v, and F_{uplift} are chosen as independent input parameters. C_{cr}, C_{ct}, C_{mr}, and η are associated with at least two of the variables mentioned above. The value ranges that are determined according to the actual operations which may be encountered are shown in Table 3.

A total of 17 sampling sets are generated by OLHS strategy. Each sampling set is calculated through FEM. The calculations take approximately 1.5 h per case on a PC (Intel® Core™ i7-8700 CPU @3.2GHz with 64GB RAM and Windows 10 64-bit system). Then, outputs of the CF in time series are obtained. After applying a 20 Hz low-pass filter advised by the standard [34] to CF, the mean value (F_m), variance (σ), maximum ($F_{\max}$) and minimum ($F_{\min}$) values are obtained. Also does the uplift displacement (U_{plift}) of CW.

3.3 Input features extraction and selection

The input features are called feature indicators (FIs). The extraction and selection of FIs form the fundamental basis for the prediction model [35]. The purpose of this step is to ex-

Table 3 Value range of independent input values

Input	T_c (kN)	T_m (kN)	v (km/h)	F_{uplift} (N)
Range	10-30	10-30	50-400	70-90

tract the key input features needed in the prediction model to reduce the intricacy of the regression and optimize the model. Due to the low initial training data size and high dimension of the input variables for the training model, this does not facilitate the accurate prediction of the GPR [12]. In this study, a wrapper method is used to implement feature selections.

Wrapper method uses specific learning algorithms to assess the quality of the selected FIs. The predictive performance is utilized to evaluate feature subsets. Typically, a predefined search process is conducted within the space of potential feature subsets, generating and evaluating various subsets. The general procedure involves selecting a subset, evaluating it based on predictive performance, selecting a new subset, and continuing the evaluation process until the desired quality is achieved. Incorporating cross-validation strategies in wrapper-based models can enhance the accuracy of the model, but it also leads to increased computational complexity and a higher risk of overfitting. The hunger games search (HGS) algorithm, proposed by Yang et al. [36], is a novel and robust meta-heuristic optimization method. Original HGS is used for continuous optimization. In this study, two modifications are implemented so that they can be applied to the FIs selection process. First is to modify the structure to deal with binary decision parameters, which details can be found in Ref. [37]. Two is to insert chaos mechanism to avert the local entrapment. The chaotic maps used in present work are shown in Table 4. In the following sections, the results obtained by this wrapper method is abbreviated as Chaos-HGS GPR (CHGS-GPR). The results with and without FIs selection are discussed in detail in the following paper.

3.4 Data preparation for training, validation and test

The purpose of this step is to normalize the input data and determine the dataset allocation for training, validation, and testing. Given the limited number of training samples used in this study, the leave-one-out cross-validation (LOO-CV) method is deemed suitable for validation. LOO-CV is a specific form of cross-validation where, in this case, one set of data is withheld as the validation reference for each training session, while the remaining 16 data sets are employed as the training datasets. In total, 17 validations are conducted. LOO-CV is particularly well-suited for datasets with a small number of samples. Furthermore, to mitigate prediction bias and enhance algorithmic stability during the learning process [39], the min-max normalization method is employed in this study. The min-max normalisation method is used here:

$$x' = \frac{x - x_{\min}}{x_{\max} - x_{\min}}, \tag{9}$$

where x is the original parameter and x' is the normalized parameter.

Once the regression model has been optimized for FIs selection and LOO-CV validation, additional test datasets are implemented to test the model. The input parameters of the test datasets vary within the range of the training data but avoid the same value as the training data. It aims to assess the generalization and predictive capability of the trained model on unseen data points.

3.5 Validation of the approach

The purpose of this step is to check the accuracy of predictions. We perform the validation by comparing the FEM results with the GPR results. Visualising the output is challenging due to the high dimensionality of the inputs. Therefore, we diagnose the prediction results using statistical measures, which are R^2, the root mean squared error (RMSE), and the mean absolute error (MAE). The definitions are shown below:

$$R^2 = 1 - \frac{\sum(y_i - \hat{y}_i)^2}{\sum(y_i - \bar{y})^2}, \tag{10}$$

$$\text{RMSE} = \sqrt{\frac{\sum(y_i - \hat{y}_i)^2}{n}}, \tag{11}$$

$$\text{MAE} = \frac{\sum \left| \frac{y_i - \hat{y}_i}{y_i} \right|}{n}, \tag{12}$$

where n is the number of data points, y_i is the true value, $\hat{y}$ is the predicted value, and $\bar{y}$ is the mean value. In simple terms,

Table 4 Chaotic maps used in the present study [38]

	Definition	Range
Circle map	$x_{k+1} = \text{mod}(x_k + b - (a - 2\pi)\sin(2\pi x_k), 1),\ a = 0.5, b = 0.2$	(0,1)
Sinusoidal map	$x_{k+1} = a x_k^2 \sin(\pi x_k)$	(0,1)
Tent map	$x_{k+1} = \begin{cases} \frac{x_k}{0.7}, & x_k < 0.7 \\ \frac{10}{3}(1 - x_k), & x_k \geq 0.7 \end{cases}$	(0,1)

R^2 is expected to be close to 1, while RMSE and MAE are required to be as small as possible, which means the approach does a good prediction.

4. Results and discussion

4.1 Model training results

Firstly, a comparison of the convergence capabilities of CHGS-GPR assembled with different chaotic maps is presented, as shown in Fig. 4. The black line represents the original random mechanism of HSG. It can be observed CHGS-GPR with tent chaotic map yields the best search performance. The optimal solution is found after five iterations. Therefore, tent map is adopted in this paper. In the following discussion, when referring to CHGS-GPR, it specifically refers to the CHGS-GPR with tent chaotic map.

Table 5 provides a comparison of the results CHGS-GPR and GPR without feature selection. From the results of R^2, RMSE, and MAE, it can be concluded that the prediction results of CHGS-GPR are better than that of the original model. It should be noted that, as to the $F_{\min}$, the proposed prediction method does not achieve satisfactory results. Its R^2 is close to zero, which means that there is almost no correlation between the input FIs and the outputs. Therefore, these results of $F_{\min}$ are not presented here. Analyzing the reason, it is not difficult to find from the time history curve of CF in Fig. 2(b) that the minimum value of the CF generally occurs when the train passes through the middle of each span of the railway, which is the position where the stiffness of the CW is the smallest. The factors that affect the stiffness of CW are probability related to the materials and configurations of CW and droppers, which is not involved in the FIs selected in the present study. In addition, small sample size may be another factor. Therefore, in the following discussion, the results related to $F_{\min}$ will not be discussed.

Then, prediction intervals are utilized to identify the potential structures in prediction errors, such as overestimating or underestimating. Figure 5 shows the relationship between LOO-CV results of CHGS-GPR and the values obtained through FEM simulations. The vertical bar represents a 95% confidence interval. The smaller the bar, the higher

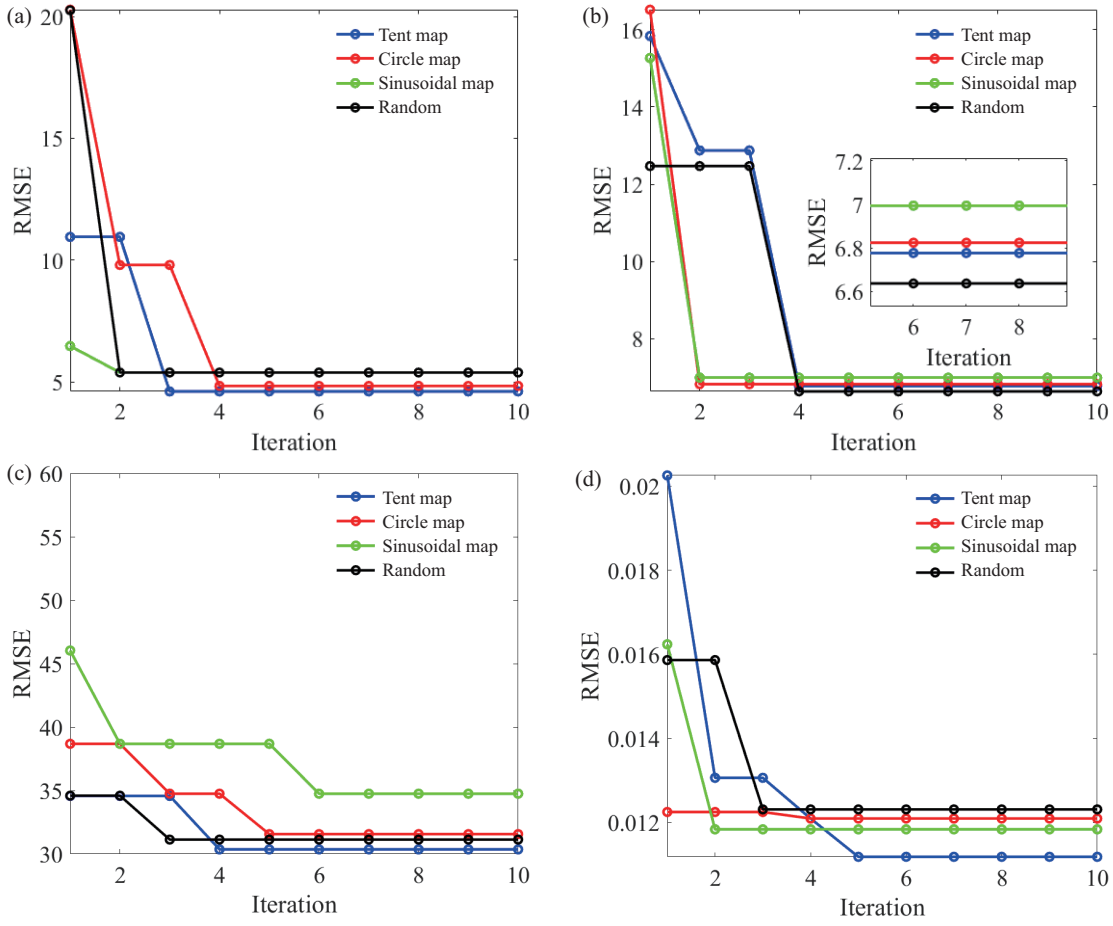

Figure 4 RMSE convergence curve for CHGS-GPR assembled with different chaotic maps. (a) F_m; (b) σ; (c) $F_{\max}$; (d) U_{plift}.

Table 5 Value range for independent input values

		FIs	R^2	RMSE	MAE
F_m	Origin	$T_c, T_m, v, F_{\text{uplift}}, C_{cr}, C_{ct}, C_{mr}, \eta$	0.984	5.38	0.029
	CHGS-GPR	$T_c, F_{\text{uplift}}, C_{mr}, \eta$	0.988	4.61	0.023
σ	Origin	$T_c, T_m, v, F_{\text{uplift}}, C_{cr}, C_{ct}, C_{mr}, \eta$	0.851	13.45	0.21
	CHGS-GPR	$T_m, F_{\text{uplift}}, C_{cr}, C_{mr}, \eta$	0.961	0.677	0.209
$F_{\max}$	Origin	$T_c, T_m, v, F_{\text{uplift}}, C_{cr}, C_{ct}, C_{mr}, \eta$	0.930	40.11	0.21
	CHGS-GPR	$T_m, F_{\text{uplift}}, C_{mr}, \eta$	0.957	30.36	0.140
U_{plift}	Origin	$T_c, T_m, v, F_{\text{uplift}}, C_{cr}, C_{ct}, C_{mr}, \eta$	0.902	0.012	0.396
	CHGS-GPR	$T_c, F_{\text{uplift}}, \eta$	0.918	0.011	0.323

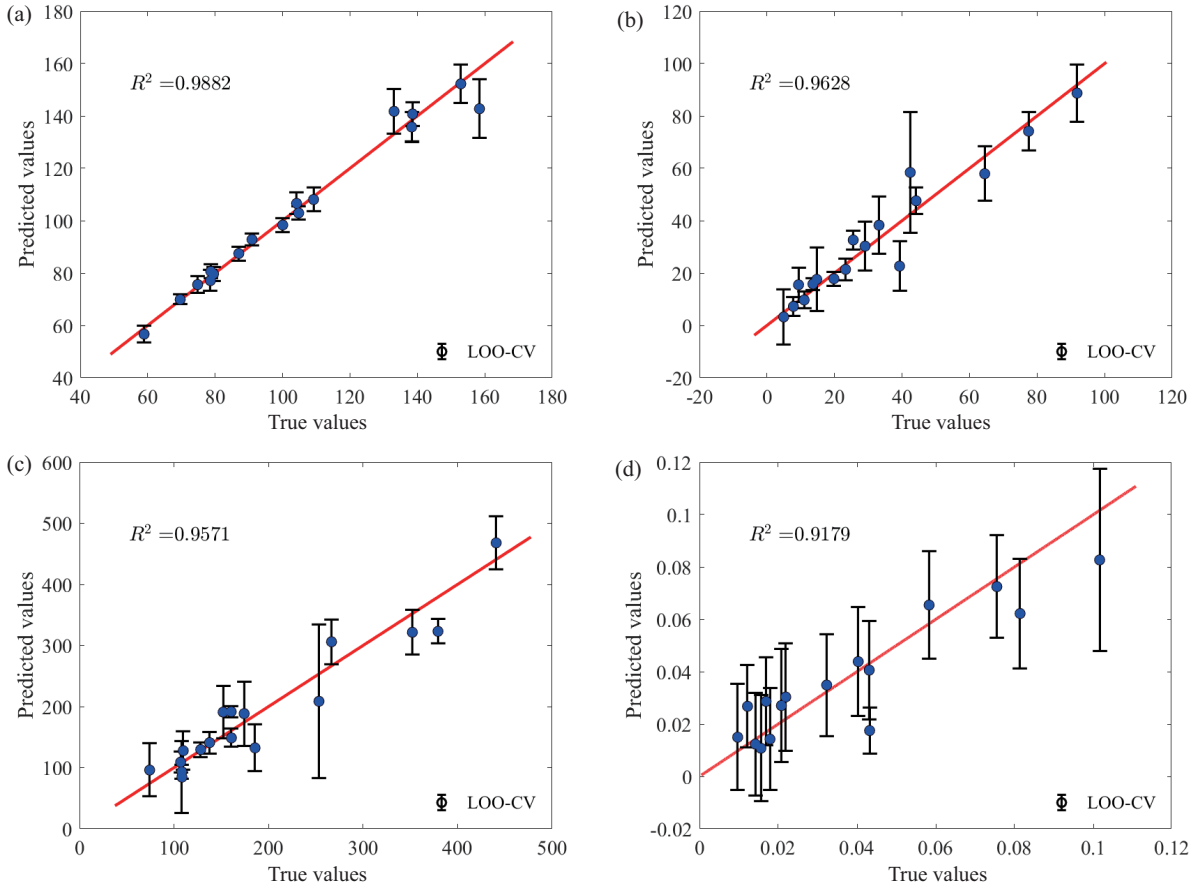

Figure 5 LOO-CV tests credible intervals results on four evaluation values of CF by CHGS-GPR. Red line is the 1:1 line, blue points are the LOO-CV results, and the bar presents 95% confidence interval. (a) F_m; (b) σ; (c) $F_{\max}$; (d) U_{plift}.

the confidence in CHGS-GPR prediction. Ideally, the midpoints of all bars would align precisely with the identification line, while having shorter bar lengths. It can be seen that the predicted values are relatively evenly distributed on both sides of the identification line (red line 1:1 in Fig. 5), indicating that there is no systematic overestimation or underestimation. Notably, the CHGS-GPR predictions of F_m exhibit the most consistent agreement with the results obtained from FEM simulations. There are some points that the CHGS-GPR returns with higher intervals, such as in Fig. 5(a) where F_m = 158 N, in Fig. 5(b) where σ = 42 N, in Fig. 5(c) where $F_{\max}$ = 253 N, and in Fig. 5(d) where U_{plift} = 0.1016 m. These points are all from the same case. Such larger prediction intervals are likely associated with the condition in this case (v = 400 km/h and η = 91%), which exceeds the commonly recommended threshold for the railway (η < 70%) [40]. Therefore, when do the LOO-CV on this set of data, the prediction intervals become larger. In summary,

the results show that CHGS-GPR does not have systematic error.

4.2 Validation and analysis

Finally, CHGS-GPR is used to predict test sample sets. R^2, RMSE, and MAE results of the test results are shown in Fig. 6. Predictions of F_m and σ perform better compared with $F_{\max}$, and U_{plift}.

Pantograph-catenary system is non-linear [41], and the default assumptions (such as the Gaussian distribution output used in GPR) may not hold, resulting in differences between FEM results and predictions. Nevertheless, as shown in Table 6, the absolute prediction error of CHGS-GPR is acceptable, especially as for the prediction of Fm performs the best. Therefore, CHGS-GPR for CF prediction used physics outputs trained proposed in this paper can be considered feasible. Considering that present results are obtained just through such a few training data sets (17 sets), it is entirely possible to obtain more accurate CHGS-GPR if the time and calculation costs increase.

5. Practical significance and prospect

The innovation and scientificity of this research lies in the application of the surrogate model based on GPR combined the optimization strategy to the prediction of CF of railway pantograph-catenary system. Unlike other machine learning models, the Gaussian process method does not require a high number of sample sets for training. At the same time, Gautam et al. [14] proved that the GPR-based machine learning model performs slightly better than the ANN-based machine learning model under the same sample size. Meanwhile, Gaussian processes can also provide a quantitative measure of the uncertainty associated with the predicted value, which is valuable in engineering applications. In the future work, more design parameters can be taken into consideration, such as pantograph operating status (knee-upstream orientation or knee-downstream orientation), railway line status (straight line, curved section or overlap), high-speed train operating environment (through tunnel, suffering horizontal wind, etc.). Increase the dimension of the input parameters to improve the integrity of the prediction model. A thorough CHGS-GPR can be integrated into computer programs to quickly establish a mapping relationship between input parameters and pantograph-catenary dynamic performance, greatly speeding up the design process. This work provides a new way of thinking for the energy transmission of high-speed railway pantograph-catenary system.

6. Conclusion

In this paper, GPR combined with meta-heuristic optimization on feature selection is used to predict the CF of the pantograph-catenary system, and its feasibility is discussed. To improve the regression, chaotic mechanism, tent map, is added to the search algorithm. FEM simulations of the pantograph-catenary system are established to generate training and testing data sets. The input variables relate to eight design parameters of the pantograph-catenary system. The output includes various statistics of CF and lifting displacement of CW. The results show that CHGS-GPR predicts well on F_m, σ, $F_{\max}$, and U_{plift}, especially F_m. However, $F_{\min}$ cannot be accurately predicted. This may be due to the fact that none of the current input parameters is the key factor affecting the minimum CF. Among them, among the input parameters, F_{uplift} and η are the most important parameters affecting pantograph-catenary transmission quality, compared with other parameters.

Among the obtained CHGS-GPR, the prediction for the Fm is the best, with R^2 = 0.997, RMSE = 2.793, and MAE = 0.0145. The outcomes obtained from CHGS-GPR using only 17 sets of training samples offer considerable reassurance. These results not only validate the feasibility of the proposed method but also demonstrate its effectiveness. This work shows the potential and viability of the approach.

The GPR model, distinguished by its probabilistic nature, exhibits remarkable suitability for probability and risk-based

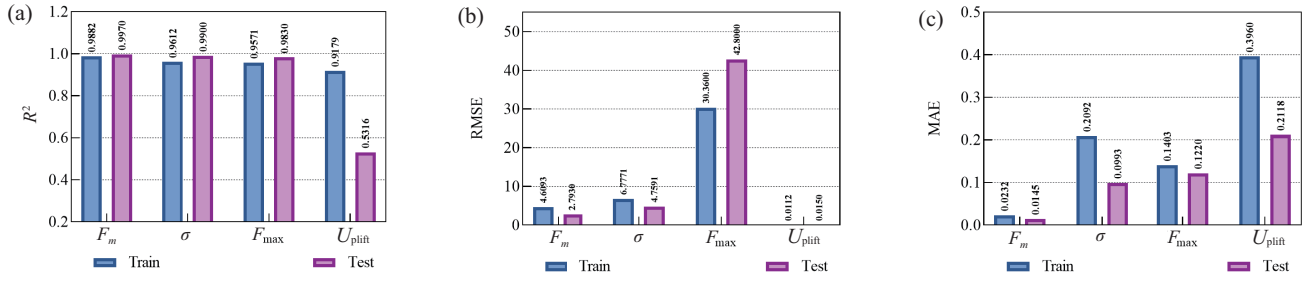

Figure 6 Model evaluation: (a) R^2, (b) RMSE, (c) MAE.

Table 6 Individual prediction error with test data set

	F_m	σ	$F_{\max}$	F_{uplift}
Absolute value of error (%)	1.45	9.93	12.2	9.02

engineering assessments, offering notable advantages in engineering prediction tasks. To the best of our knowledge, for the first time, GPR is introduced into the pantograph-catenary system, and its feasibility is discussed. The established method demonstrates acceptable accuracy and efficiency, surpassing FEM methods and potentially even replacing costly field tests for evaluating the pantograph-catenary interaction. These findings contribute to the advancement of engineering practices and offer new possibilities for enhancing system evaluation methodologies.

Appendix A.

Appendix A shows the derivation of the key dimensionless coefficients (C_{cr}, C_{ct}, and C_{mr}) related to the catenary structure around the dropper as shown in Fig. A1. The excitation is assumed to be the incident wave D. When D meets the dropper, the reflection wave A and transmission wave B will be generated on the CW. Meanwhile, the wave will be transmitted to MW through the dropper and separated into two directions, which is reflection wave E and F. Hence, the reflection and transmission coefficients are defined as the amplitude ratios between the generated wave and incident wave, which reflect the natural properties of the special segment of the catenary structure.

For catenary CW and MW, they are modelled as tensioned cables, the governing equations are as follows:

$$\rho\frac{\partial^2 w(x,t)}{\partial t^2} - T\frac{\partial^2 w(x,t)}{\partial x^2} = 0, \tag{a1}$$

where ρ is the linear density, T is the tension, and $w(x,t)$ is the vertical deflection.

As for the section around dropper, the equilibrium equation of MW and CW is as follows:

$$\begin{cases} w_{ml} = w_{mr}, \\ T_m\left(\dfrac{\partial w_{mr}}{\partial x} - \dfrac{\partial w_{ml}}{\partial x}\right) - k(w_{mr} - w_{cr}) = 0, \\ w_{cl} = w_{cr}, \\ T_c\left(\dfrac{\partial w_{cr}}{\partial x} - \dfrac{\partial w_{cl}}{\partial x}\right) + k(w_{mr} - w_{cr}) = 0, \end{cases} \tag{a2}$$

where the subscript m presents for MW and c for CW, l for the left and r for the right, and k is the spring stiffness of the dropper. The Fourier transform of the solu-tion of Eq. (a1) is as follows:

$$w(x,t) = \sum_n [w_n(x,\omega_n)\mathrm{e}^{\mathrm{i}\omega_n t}], \tag{a3}$$

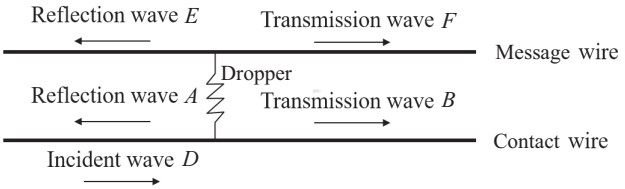

Figure A1 Schematic diagram of wave propagation around the dropper of the catenary, which A, B, D, E, and F mean the amplitude of the wave.

where ω is angular frequency. For short, Eq. (a3) can be written as

$$w(x,t) = \hat{w}(x,\omega)\mathrm{e}^{\mathrm{i}\omega t}, \tag{a4}$$

$$w(x,t) \Rightarrow \hat{w}(x,\omega). \tag{a5}$$

The form of solution of Eq. (a2) is as follows:

$$\begin{cases} \hat{w}_{ml} = E\mathrm{e}^{\mathrm{i}\omega x/c_m}, \\ \hat{w}_{mr} = F\mathrm{e}^{-\mathrm{i}\omega x/c_m}, \\ \hat{w}_{cl} = A\mathrm{e}^{\mathrm{i}\omega x/c_c} + D\mathrm{e}^{-\mathrm{i}\omega x/c_c}, \\ \hat{w}_{cr} = B\mathrm{e}^{-\mathrm{i}\omega x/c_c}. \end{cases} \tag{a6}$$

Substituting Eq. (a6) into Eq. (a2), then get

$$\frac{A}{D} = -\frac{\gamma_c}{\gamma_c + \gamma_m + i}, \tag{a7}$$

$$\frac{B}{D} = \frac{\gamma_m + i}{\gamma_c + \gamma_m + i}, \tag{a8}$$

$$\frac{E}{D} = \frac{\gamma_m}{\gamma_c + \gamma_m + i}. \tag{a9}$$

Modulo the above results as follows:

$$c_{cr} = \left|\frac{A}{D}\right| = \frac{\gamma_c}{\sqrt{(\gamma_c + \gamma_m)^2 + 1}}, \tag{a10}$$

$$c_{ct} = \left|\frac{B}{D}\right| = \frac{\sqrt{(\gamma_m^2 + \gamma_m\gamma_c + 1)^2 + \gamma_c^2}}{(\gamma_c + \gamma_m)^2 + 1}, \tag{a11}$$

$$c_{mr} = \left|\frac{E}{D}\right| = c_{mt} = \frac{\gamma_m}{\sqrt{(\gamma_c + \gamma_m)^2 + 1}}, \tag{a12}$$

where γ_m and γ_c are defined as

$$\gamma_m = \frac{k}{2\omega\sqrt{\rho_m T_m}}, \tag{a13}$$

$$\gamma_c = \frac{k}{2\omega\sqrt{\rho_c T_c}}. \tag{a14}$$

As can been seen, C_{cr}, C_{ct}, and C_{mr} are the reflection coefficients of CW, transmission coefficients of CW and reflection coefficient of MW, respectively.

Conflict of interest *On behalf of all authors, the corresponding author states that there is no conflict of interest.*

Author contributions *Mohan Zhang did the conceptualization part and wrote the draft. Bo Yin and Zhenxu Sun reviewed and edited the draft. Ye Bai helped organize the manuscript. Guowei Yang supported the funding and edited the final version.*

Acknowledgements *This work was supported by the China National Railway Group Science and Technology Program (Grant No. N2022T001)*

1 IEC 62486, Railway applications—current collection systems—Technical criteria for the interaction between pantograph and overhead contact line, 2017.

2 A. Kampczyk, and K. Dybeł, The fundamental approach of the digital twin application in railway turnouts with innovative monitoring of weather conditions, Sensors **21**, 5757 (2021).

3 A. Meixedo, J. Santos, D. Ribeiro, R. Calçada, and M. Todd, Damage detection in railway bridges using traffic-induced dynamic responses, Eng. Struct. **238**, 112189 (2021).

4 M. Hamarat, M. Papaelias, and S. Kaewunruen, Fatigue damage assessment of complex railway turnout crossings via Peridynamics-based digital twin, Sci. Rep. **12**, 14377 (2022).

5 R. Jiang, W. Wang, Y. Xie, and X. Yin, in Research and design of infrastructure monitoring platform of intelligent high speed railway: Proceedings of 2022 IEEE 6th Information Technology and Mechatronics Engineering Conference (ITOEC), (IEEE, 2022), pp. 2096-2099.

6 R. Kulkarni, A. De Rosa, A. Qazizadeh, M. Berg, E. Di Gialleonardo, A. Facchinetti, and S. Bruni, Monitoring of Alignment Level (AL) and Cross Level (CL) track geometry irregularities from onboard vehicle dynamics measurements using probabilistic fault classifier, in: Advances in Dynamics of Vehicles on Roads and Tracks II: Proceedings of the 27th Symposium of the International Association of Vehicle System Dynamics, IAVSD 2021, Saint Petersburg, (Springer, 2022), pp. 479-487.

7 Y. Li, W. Zhang, Q. Xiong, T. Lu, and G. Mei, A novel fault diagnosis model for bearing of railway vehicles using vibration signals based on symmetric alpha-stable distribution feature extraction, Shock Vib. **2016**, 5714195 (2016).

8 M. Kreuzer, A. Schmidt, and W. Kellermann, in Novel features for the detection of bearing faults in railway vehicles: Proceedings of INTER-NOISE and NOISE-CON Congress and Conference, Institute of Noise Control Engineering, 2021, pp. 3833-3844.

9 M. Jesussek, and K. Ellermann, Fault detection and isolation for a full-scale railway vehicle suspension with multiple Kalman filters, Veh. Syst. Dyn. **52**, 1695 (2014).

10 X. Wei, L. Jia, K. Guo, and S. Wu, On fault isolation for rail vehicle suspension systems, Veh. Syst. Dyn. **52**, 847 (2014).

11 G. Huang, G. Wu, Z. Yang, X. Chen, and W. Wei, Development of surrogate models for evaluating energy transfer quality of high-speed railway pantograph-catenary system using physics-based model and machine learning, Appl. Energy **333**, 120608 (2023).

12 R. Hejazi, A. Grime, M. Randolph, and M. Efthymiou, A Bayesian machine learning approach to rapidly quantifying the fatigue probability of failure for steel catenary risers, Ocean Eng. **235**, 109353 (2021).

13 M. Alruqi, P. Sharma, B. Deepanraj, and F. Shaik, Renewable energy approach towards powering the CI engine with ternary blends of algal biodiesel-diesel-diethyl ether: Bayesian optimized Gaussian process regression for modeling-optimization, Fuel **334**, 126827 (2023).

14 Gautam, K. K. Gupta, D. Bhowmik, and S. Dey, Probing the stochastic unconfined compressive strength of lime-RHA mix treated clayey soil, J. Mater. Civ. Eng. **35**, 04022469 (2023).

15 A. Gelman, and C. R. Shalizi, Philosophy and the practice of Bayesian statistics, Br. J. Math. Stat. Psychol. **66**, 8 (2013).

16 N. Zhou, Q. Lv, Y. Yang, and W. Zhang, Statement of methods, Veh. Syst. Dyn. **53**, 380 (2015).

17 M. Tur, L. Baeza, F. J. Fuenmayor, and E. García, PACDIN statement of methods, Veh. Syst. Dyn. **53**, 402 (2015).

18 C. Sánchez-Rebollo, A. Carnicero, and J. R. Jiménez-Octavio, CANDY statement of methods, Veh. Syst. Dyn. **53**, 392 (2015).

19 J. P. Massat, E. Balmes, J. P. Bianchi, and G. Van Kalsbeek, OSCAR statement of methods, Veh. Syst. Dyn. **53**, 370 (2015).

20 P. A. Jönsson, S. Stichel, and C. Nilsson, CaPaSIM statement of methods, Veh. Syst. Dyn. **53**, 341 (2015).

21 M. Ikeda, "Gasen-do FE" statement of methods, Veh. Syst. Dyn. **53**, 357 (2015).

22 A. Collina, S. Bruni, A. Facchinetti, and A. Zuin, PCaDA statement of methods, Veh. Syst. Dyn. **53**, 347 (2015).

23 Y. H. Cho, SPOPS statement of methods, Veh. Syst. Dyn. **53**, 329 (2015).

24 J. Ambrósio, J. Pombo, P. Antunes, and M. Pereira, PantoCat statement of method, Veh. Syst. Dyn. **53**, 314 (2015).

25 Dassault Systémes. Abaqus theory guide.

26 S. Bruni, J. Ambrosio, A. Carnicero, Y. H. Cho, L. Finner, M. Ikeda, S. Y. Kwon, J. P. Massat, S. Stichel, M. Tur, and W. Zhang, The results of the pantograph-catenary interaction benchmark, Veh. Syst. Dyn. **53**, 412 (2015).

27 BS EN 50119, Railway applications—fixed installations—electric traction overhead contact lines, 2020.

28 BS EN 50317, Railway applications—current collection systems—requirements for and validation of measurements of the dynamic interaction between pantograph and overhead contact line, 2012.

29 CEI EN 50367, Railway applications—current collection systems—technical criteria for the interaction between pantograph and overhead line (to achieve free access), 2012.

30 Y. Song, Z. Liu, F. Duan, Z. Xu, and X. Lu, Wave propagation analysis in high-speed railway catenary system subjected to a moving pantograph, Appl. Math. Model. **59**, 20 (2018).

31 O. Vo Van, J. P. Massat, and E. Balmes, Waves, modes and properties with a major impact on dynamic pantograph-catenary interaction, J. Sound Vib. **402**, 51 (2017).

32 M. Zhao, and W. C. Cui, Application of the optimal Latin hypercube design and radial basis function network to collaborative optimization, J. Mar. Sci. Appl. **6**, 24 (2007).

33 J. S. Park, Optimal Latin-hypercube designs for computer experiments, J. Stat. Plan. Inference **39**, 95 (1994).

34 EN 50318, European committee for railway applications—current collection systems—validation of simulation of the dynamic interaction between pantograph and overhead contact line, 2002.

35 X. Hu, Y. Che, X. Lin, and S. Onori, Battery health prediction using fusion-based feature selection and machine learning, IEEE Trans. Transp. Electrific. **7**, 382 (2021).

36 Y. Yang, H. Chen, A. A. Heidari, and A. H. Gandomi, Hunger games search: Visions, conception, implementation, deep analysis, perspectives, and towards performance shifts, Expert Syst. Appl. **177**, 114864 (2021).

37 R. Manjula Devi, M. Premkumar, P. Jangir, B. Santhosh Kumar, D. Alrowaili, and K. Sooppy Nisar, BHGSO: Binary hunger games search optimization algorithm for feature selection problem, Comput. Mater. Contin. **70**, 557 (2022).

38 C. J. Burnett, C. Li, E. Webber, E. Tsaousidou, S. Y. Xue, J. C. Brüning, and M. J. Krashes, Hunger-driven motivational state competition, Neuron **92**, 187 (2016).

39 K. P. Murphy, A Probabilistic Perspective (MIT Press, Cambridge, 2012).
40 F. Kiessling, R. Puschmann, and A. Schmieder, Contact Lines for Electric Railways: Planning, Design, Implementation, Maintenance (Publicis Corporate Publishing, Paris, 2018).
41 Y. H. Cho, Numerical simulation of the dynamic responses of railway overhead contact lines to a moving pantograph, considering a nonlinear dropper, J. Sound Vib. **315**, 433 (2008).

应用元启发式优化和高斯过程回归预测受电弓-接触网系统性能的可行性研究

张莫晗, 银波, 孙振旭, 白夜, 杨国伟

摘要 受电弓接触网系统为高速列车提供电能, 正确评估受电弓与接触网之间的接触力(CF)对于稳定供电至关重要. CF的大小和变化范围决定了列车受流质量和安全运行. 因此, 快速、准确地预测CF具有重要意义. 然而, 通过实验收集CF数据具有挑战性, 并且通过数值模拟获得及时结果并不总是可行的. 在本研究中, 我们提出了一种结合元启发式优化和高斯过程回归的高效的代理模型方法, 来预测受电弓接触网系统接触力统计量. 首先, 使用有限元法(FEM)建立并验证受电弓接触网模型, 用于生成训练和测试数据集. 其次, 利用高斯过程回归(GPR)进行对接触力的预测. 将一种新开发的元启发式优化, 即二元饥饿游戏搜索(HGS), 应用于特征选择. 为了增强BHGS的性能, 嵌入了混沌机制, 产生了Chaos-HGS GPR(CHGS-GPR). 最后, 对CHGS-GPR的预测结果进行了评估. 结果发现, 所提出的CHGS-GPR对CF的平均值提供了相当准确的预测, 并且可以扩展到铁路线路的初步设计、列车运行的实时评估和控制.